Supporting Information for

Large-scale Statistically Meaningful Patterns (LSMPs) associated with precipitation extremes over Northern California

Abhishekh Kumar Srivastava[1*], Richard Grotjahn[1], Alan M. Rhoades[2], Paul Aaron Ullrich[1,3]

[1]Department of Land, Air and Water Resources, University of California, Davis, CA, USA
[2]Lawrence Berkeley National Laboratory, Berkeley, CA, USA
[3]Lawrence Livermore National Laboratory, Livermore, CA, USA

Contents of this file:

[*]Department of Land, Air and Water Resources, University of California, Davis, CA, USA

Corresponding author: Abhishekh Kumar Srivastava, asrivas@ucdavis.edu

Table S1: Prediction skills in capturing observed extreme precipitation events ($> 95^{th}$ percentile) using LSMP indices (LSMPis) as predictors constructed for daily meteorological fields at lags 0 and 2 (in parenthesis). POD: probability of detection. FAR: false alarm ratio. TS: threat score. GSS: Gilbert skill score. PSS: Pierce skill score. AIC: Akaike Information Criteria. Training period: NDJFM of 1948-1982; verification period: NDJFM of 1982-2015. The variables shown are anomalies but the subscript 'a' has been removed for brevity here.

Data	hits	misses	FA	CN	POD	FAR	TS	GSS	PSS	AIC
					IVT					
Training	217 (190)	27 (54)	762 (1387)	4136 (3509)	0.89 (0.78)	0.78 (0.88)	0.22 (0.12)	0.18 (0.07)	0.73 (0.5)	37373 (40789)
Verification	213 (196)	32 (49)	996 (1530)	3750 (3214)	0.87 (0.8)	0.82 (0.89)	0.17 (0.11)	0.13 (0.07)	0.66 (0.48)	36111 (38485)
					PW					
Training	217 (190)	27 (54)	998 (1419)	3900 (3477)	0.89 (0.78)	0.82 (0.88)	0.17 (0.11)	0.13 (0.07)	0.69 (0.49)	38523 (41323)
Verification	209 (167)	36 (78)	1227 (1524)	3519 (3220)	0.85 (0.68)	0.85 (0.9)	0.14 (0.09)	0.1 (0.05)	0.59 (0.36)	37280 (39505)
					U850					
Training	215 (188)	29 (56)	1128 (1510)	3770 (3386)	0.88 (0.77)	0.84 (0.89)	0.16 (0.11)	0.12 (0.06)	0.65 (0.46)	39329 (41166)
Verification	205 (189)	40 (56)	1241 (1462)	3505 (3282)	0.84 (0.77)	0.86 (0.89)	0.14 (0.11)	0.09 (0.07)	0.58 (0.46)	37505 (38621)
					SLP					
Training	209 (173)	35 (71)	1122 (1595)	3776 (3301)	0.86 (0.71)	0.84 (0.9)	0.15 (0.09)	0.11 (0.05)	0.63 (0.38)	39654 (42108)
Verificatio	204 (175)	41 (70)	1227 (1443)	3519 (3301)	0.83 (0.71)	0.86 (0.89)	0.14 (0.1)	0.1 (0.06)	0.57 (0.41)	37350 (39438)
					Z500					
Training	212 (175)	32 (69)	1261 (1649)	3637 (3247)	0.87 (0.72)	0.86 (0.9)	0.14 (0.09)	0.1 (0.05)	0.61 (0.38)	39895 (42154)
Verification	205 (181)	40 (64)	1276 (1556)	3470 (3188)	0.84 (0.74)	0.86 (0.9)	0.13 (0.1)	0.09 (0.06)	0.57 (0.41)	37623 (39415)
					V850					
Training	205 (186)	39 (58)	1121 (1529)	3777 (3367)	0.84 (0.76)	0.85 (0.89)	0.15 (0.1)	0.11 (0.06)	0.61 (0.45)	39949 (41751)
Verification	200 (170)	45 (75)	1368 (1569)	3378 (3175)	0.82 (0.69)	0.87 (0.9)	0.12 (0.09)	0.08 (0.05)	0.53 (0.36)	38219 (39377)
					T500					
Training	188 (154)	56 (90)	1431 (1732)	3467 (3164)	0.77 (0.63)	0.88 (0.92)	0.11 (0.08)	0.07 (0.03)	0.48 (0.28)	41175 (42732)
Verification	181 (155)	64 (90)	1793 (1939)	2953 (2805)	0.74 (0.63)	0.91 (0.93)	0.09 (0.07)	0.04 (0.03)	0.36 (0.22)	39368 (40430)
					Ts					
Training	186 (144)	58 (100)	1679 (1891)	3219 (3005)	0.76 (0.59)	0.9 (0.93)	0.1 (0.07)	0.05 (0.02)	0.42 (0.2)	41376 (43054)
Verification	194 (127)	51 (118)	1829 (1817)	2917 (2927)	0.79 (0.52)	0.9 (0.93)	0.09 (0.06)	0.05 (0.02)	0.41 (0.14)	39196 (40733)
					T850					
Training	186 (149)	58 (95)	1555 (1758)	3343 (3138)	0.76 (0.61)	0.89 (0.92)	0.1 (0.07)	0.06 (0.03)	0.44 (0.25)	41419 (42871)
Verification	196 (142)	49 (103)	1794 (2025)	2952 (2719)	0.8 (0.58)	0.9 (0.93)	0.1 (0.06)	0.05 (0.02)	0.42 (0.15)	39192 (40633)

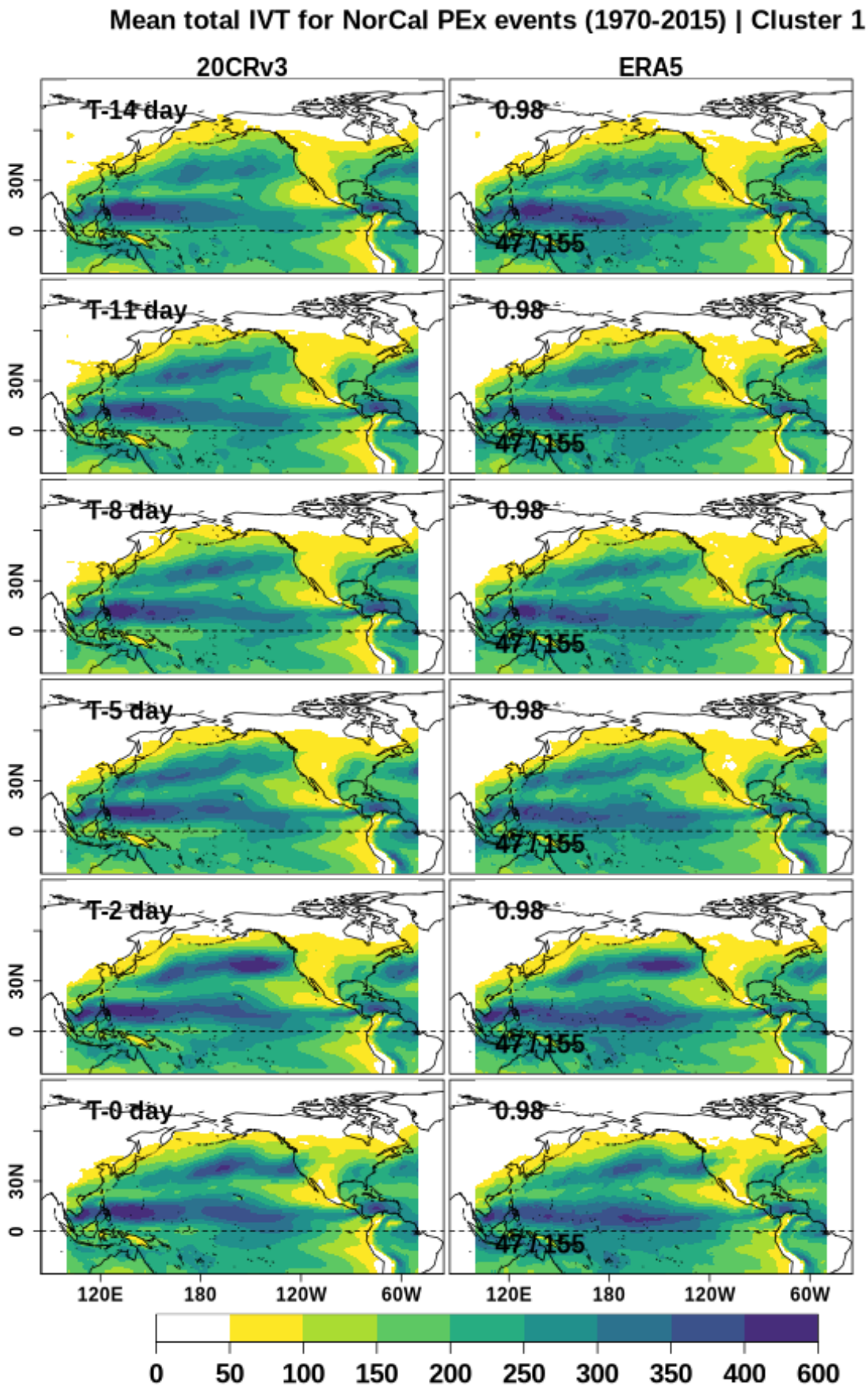

Figure S1: The evolution of total integrated vapor transport (IVT) for cluster 1 (shading; unit: kg/m-s). The ratio in the right panel shows the number of events in that cluster divided by the total number of events. The numbers on the upper-left in the right panels indicate the correlation between the two datasets. Left panel: 20CRv3. Right Panel: ERA5

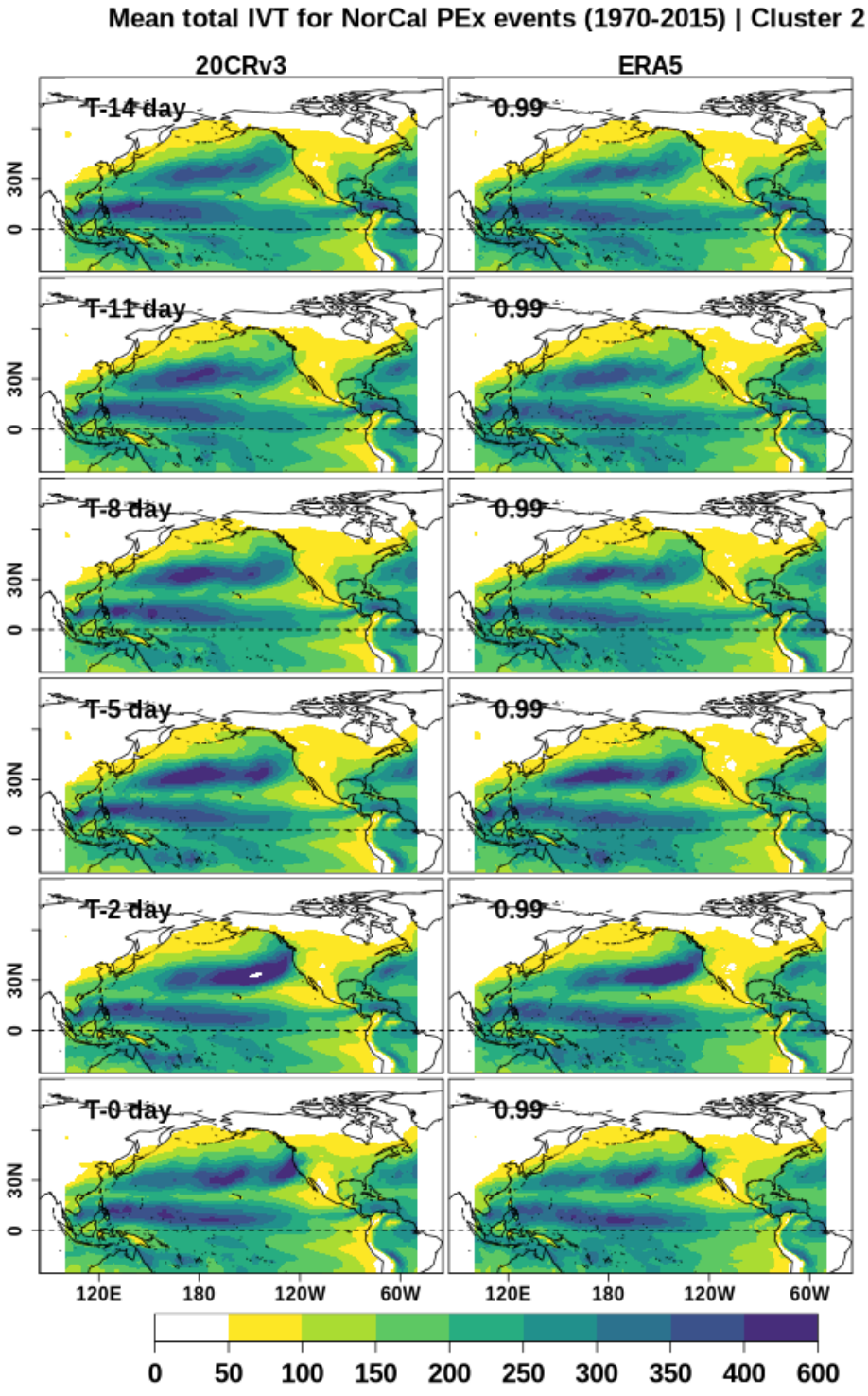

Figure S2: Same as in Fig. S1 but for cluster 2.

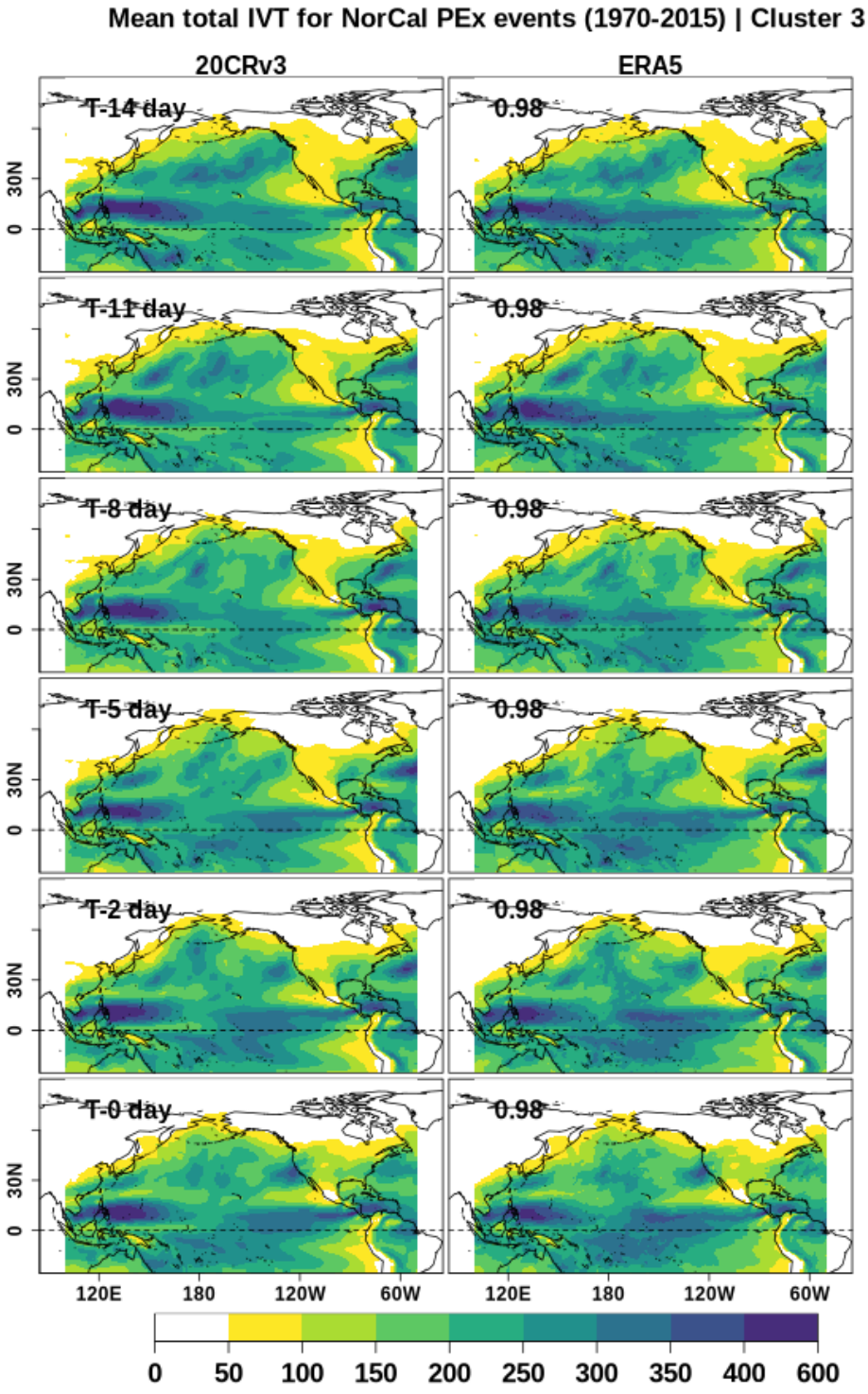

Figure S3: Same as in Fig. S1 but for cluster 3.

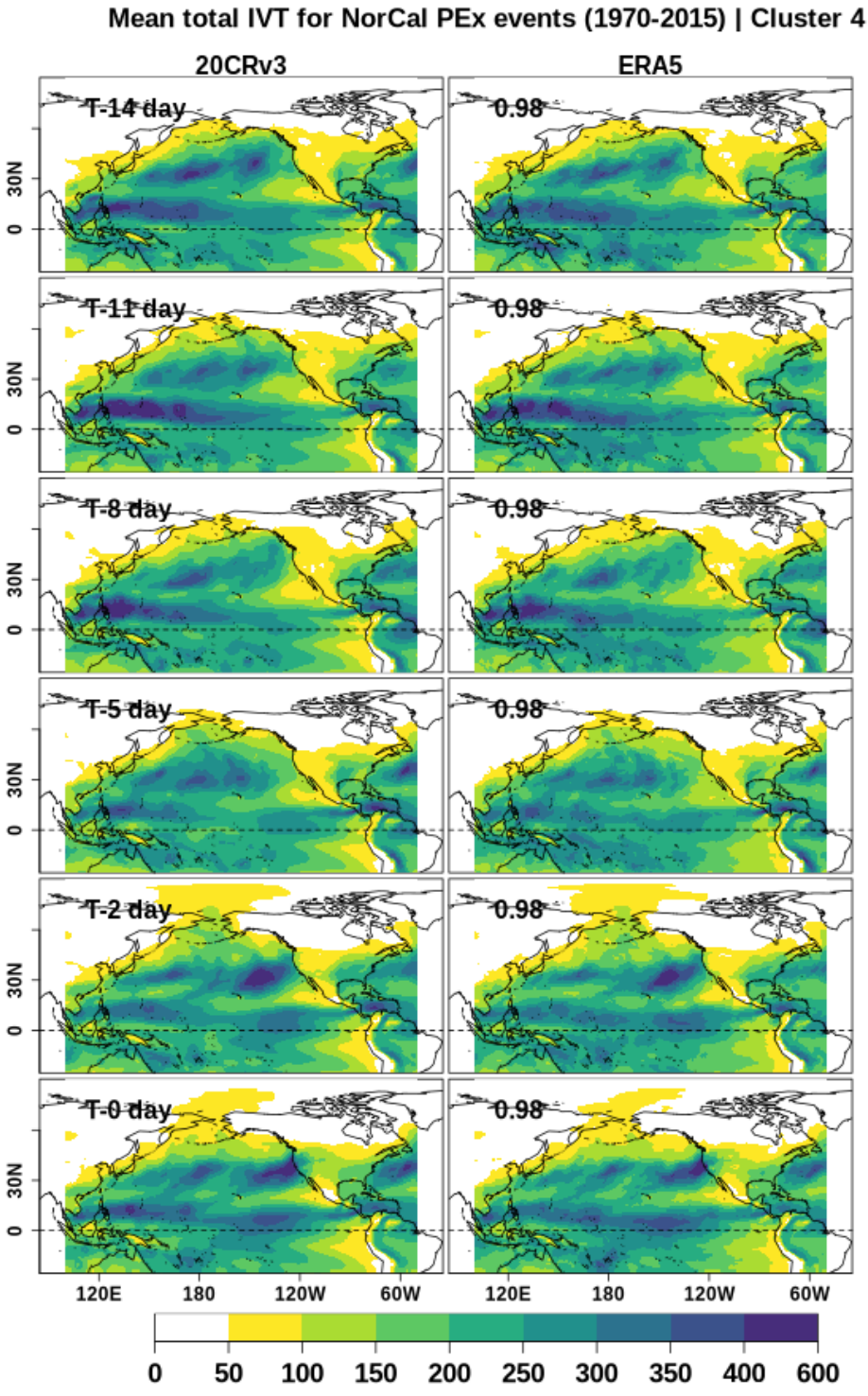

Figure S4: Same as in Fig. S1 but for cluster 4.

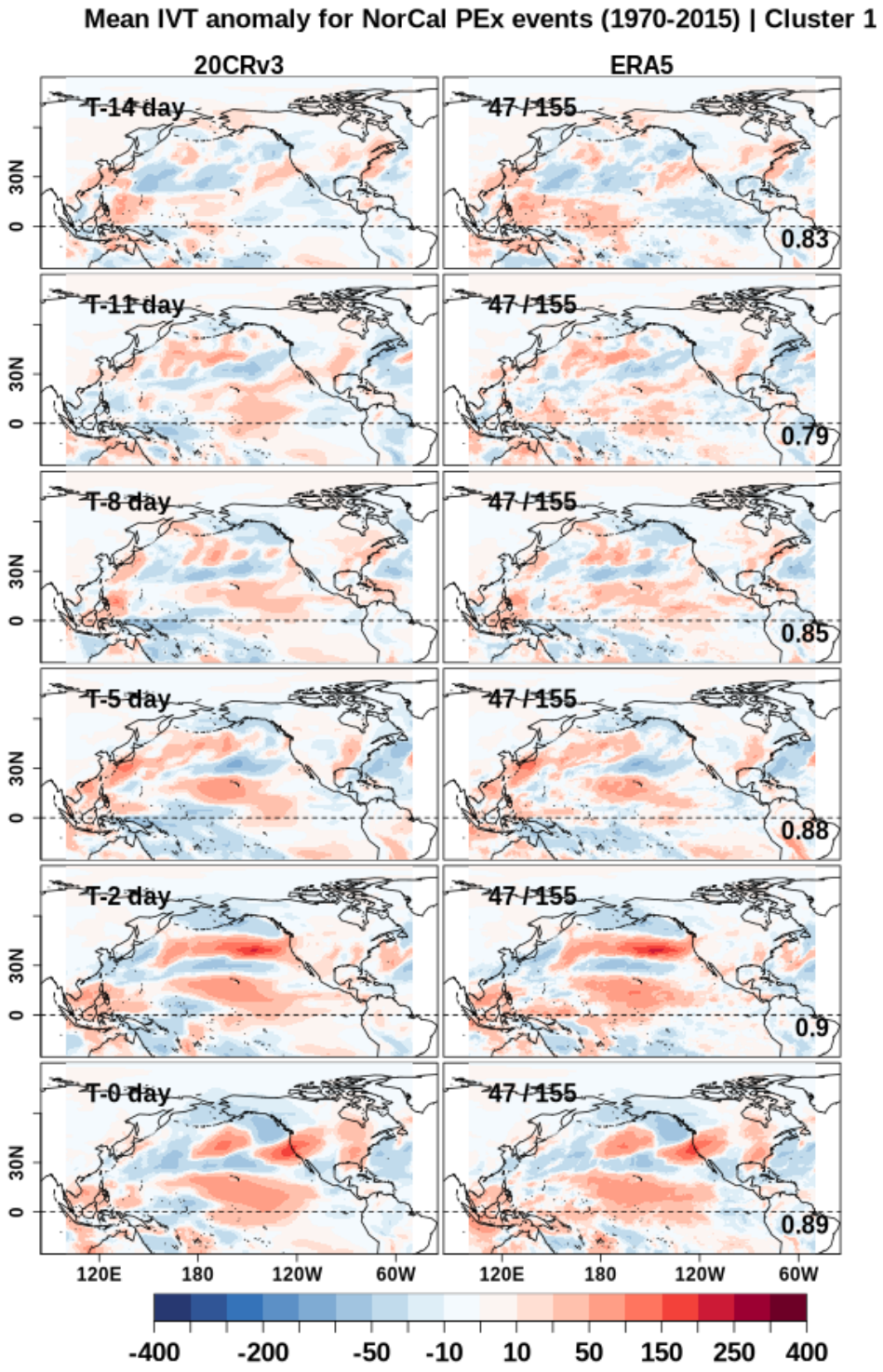

Figure S5: The evolution of integrated vapor transport anomalies for cluster 1 (shading; unit: kg/m-s). The ratio in the right panel shows the number of events in that cluster divided by the total number of events. The numbers on the lower-right in the right panels indicate the correlation between the two datasets. Left panel: 20CRv3. Right Panel: ERA5

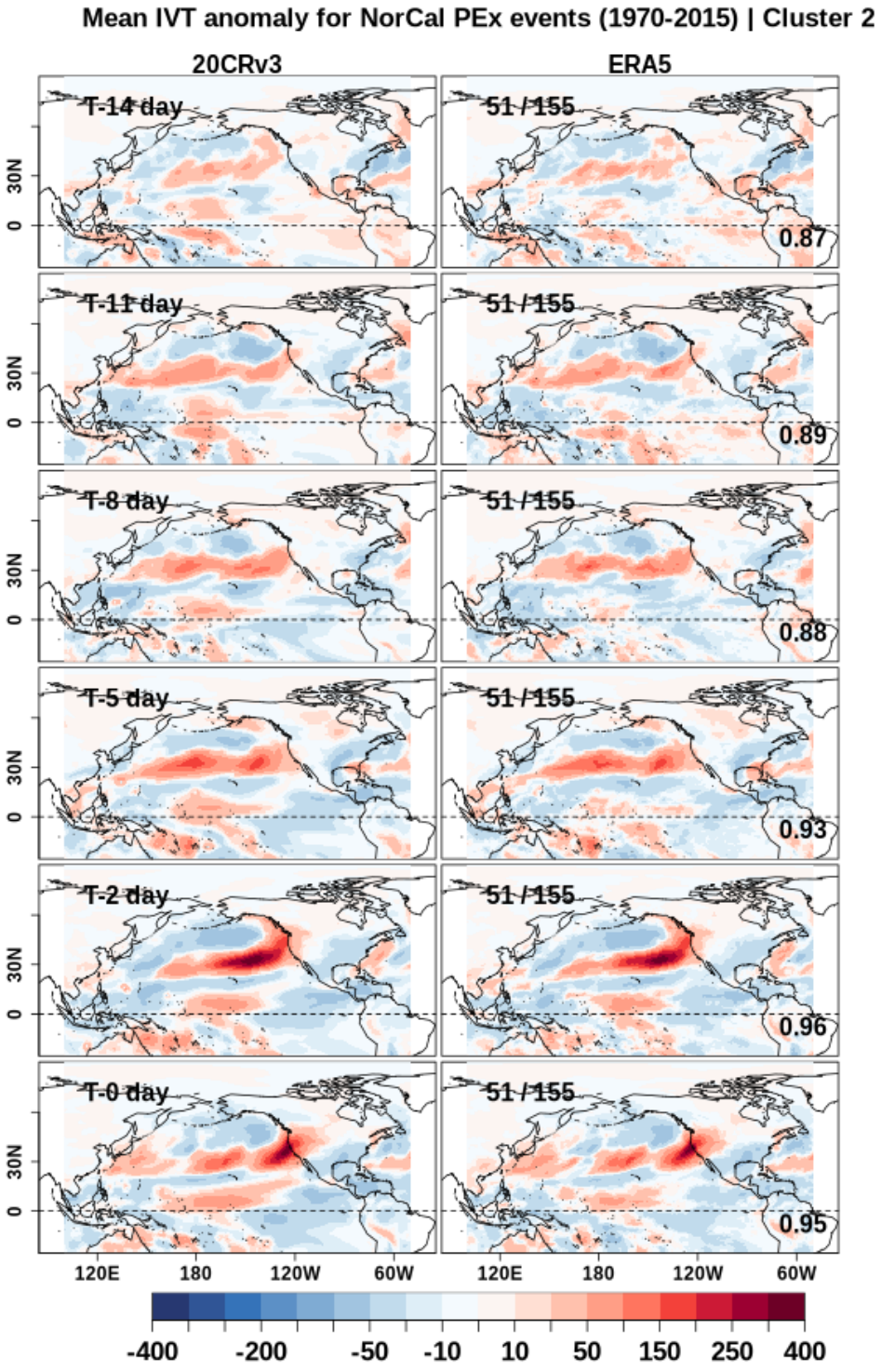

Figure S6: Same as in Fig. S5 but for cluster 2.

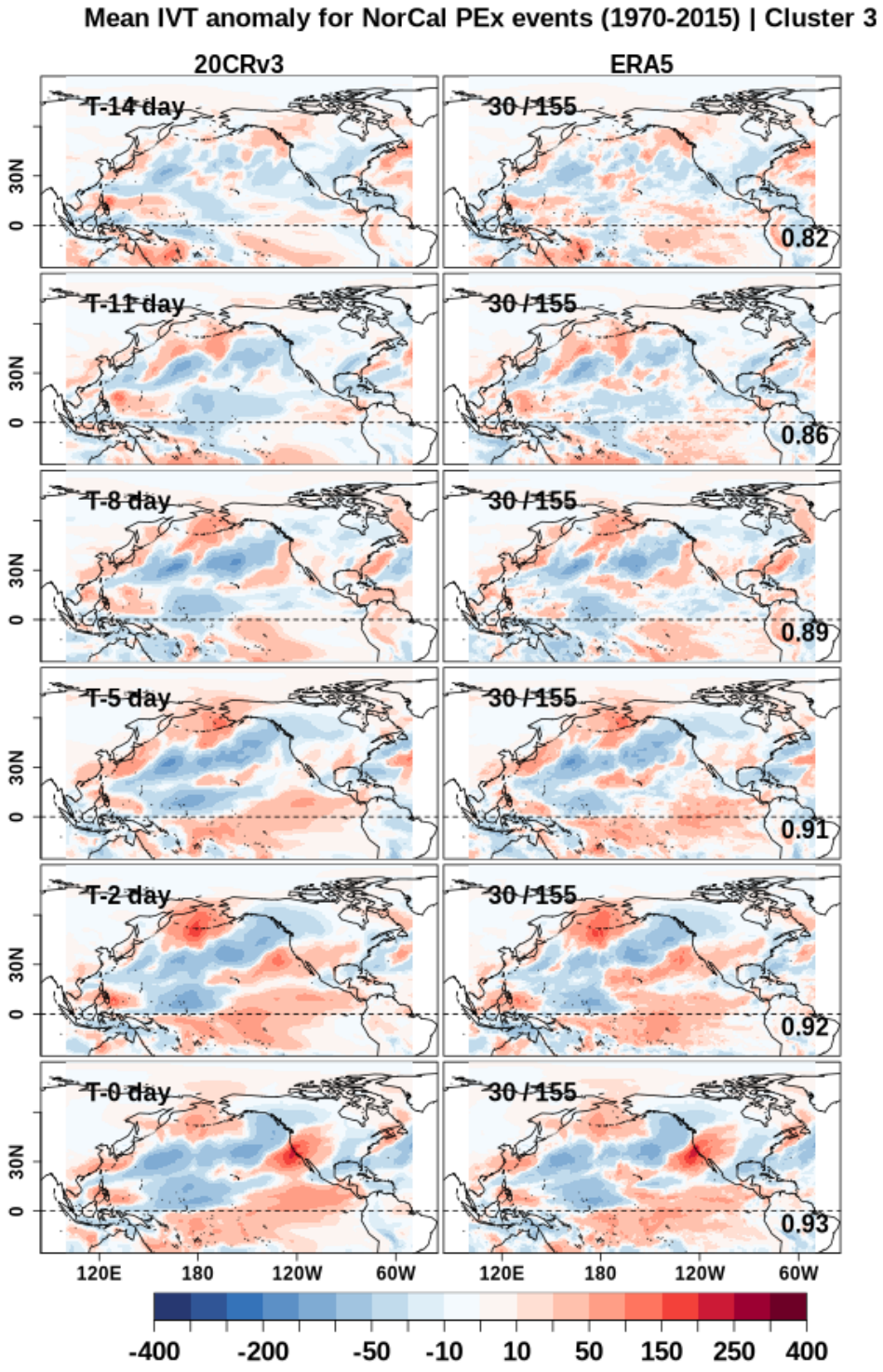

Figure S7: Same as in Fig. S5 but for cluster 3.

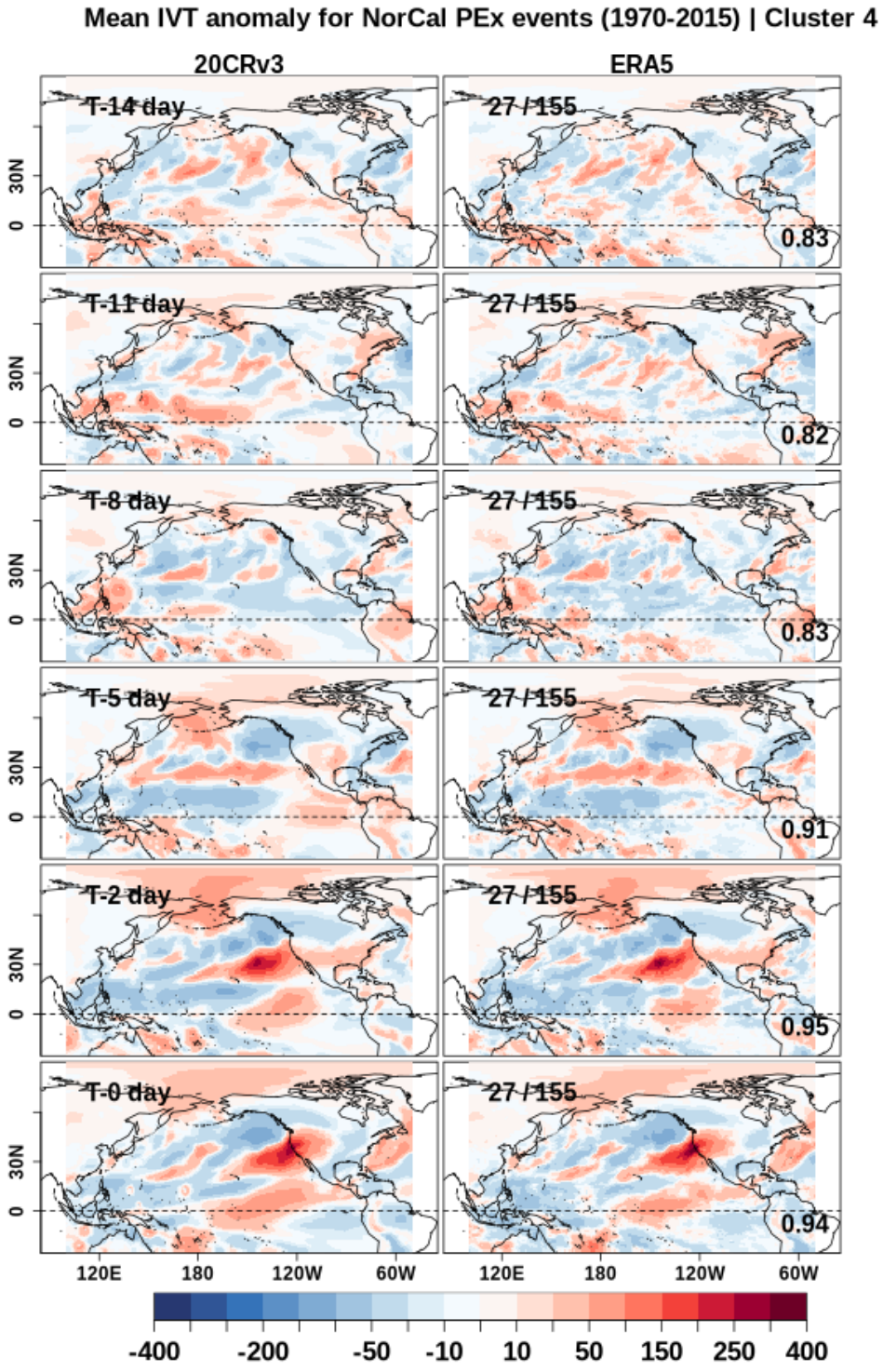

Figure S8: Same as in Fig. S5 but for cluster 4.

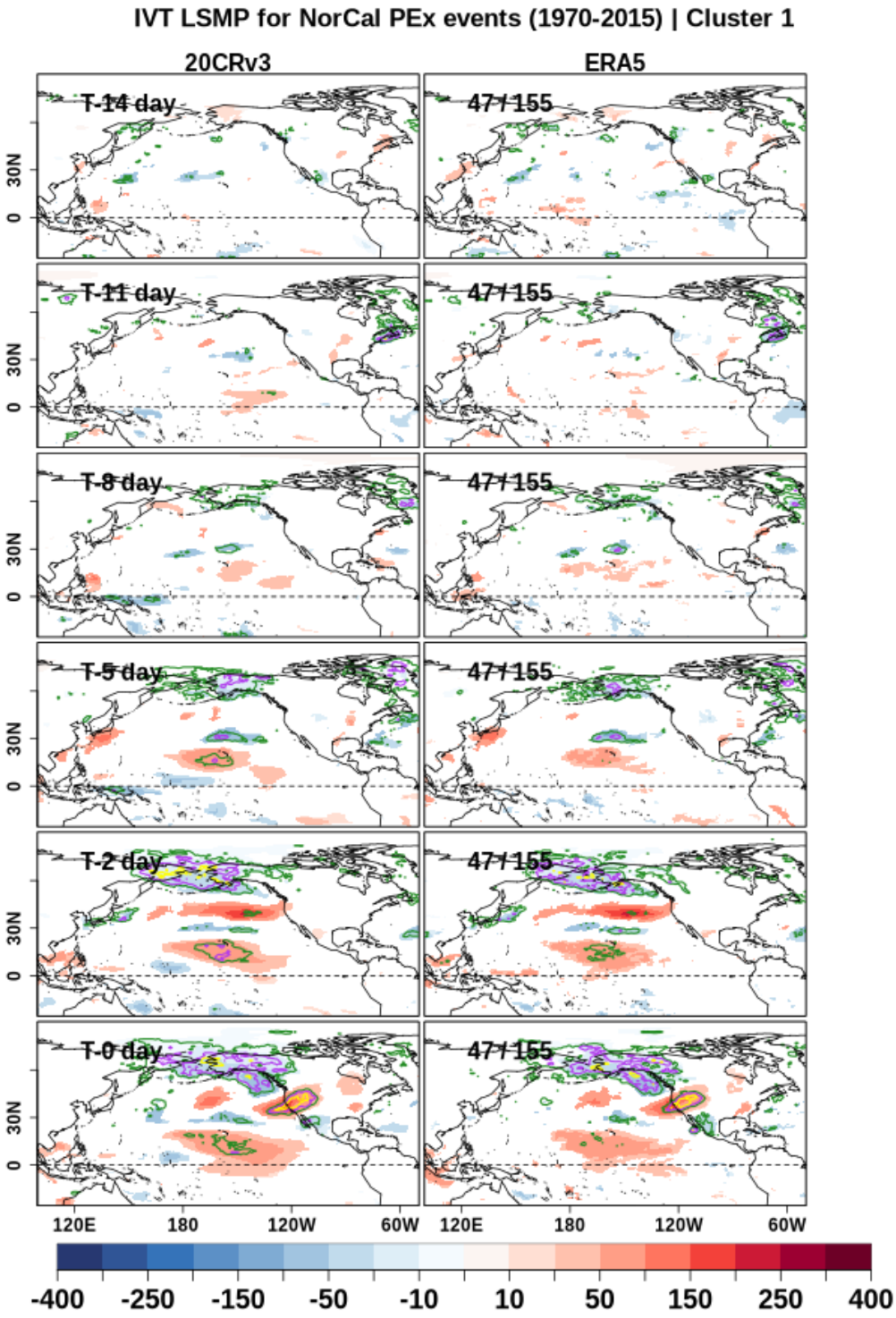

Figure S9: The evolution of integrated vapor transport anomalies (IVT LSMPs) for cluster 1 (shading; unit: kg/m-s). Shaded areas show anomalies significant at the 5% level. Contours show the consistency of the anomaly pattern. Green, magenta and yellow contours show that at least 80%, 87.5%, and 95% of the cluster members have the same sign of anomalies, respectively. The ratio in the right panel shows the number of events in that cluster divided by the total number of events. Left panel: 20CRv3. Right Panel: ERA5

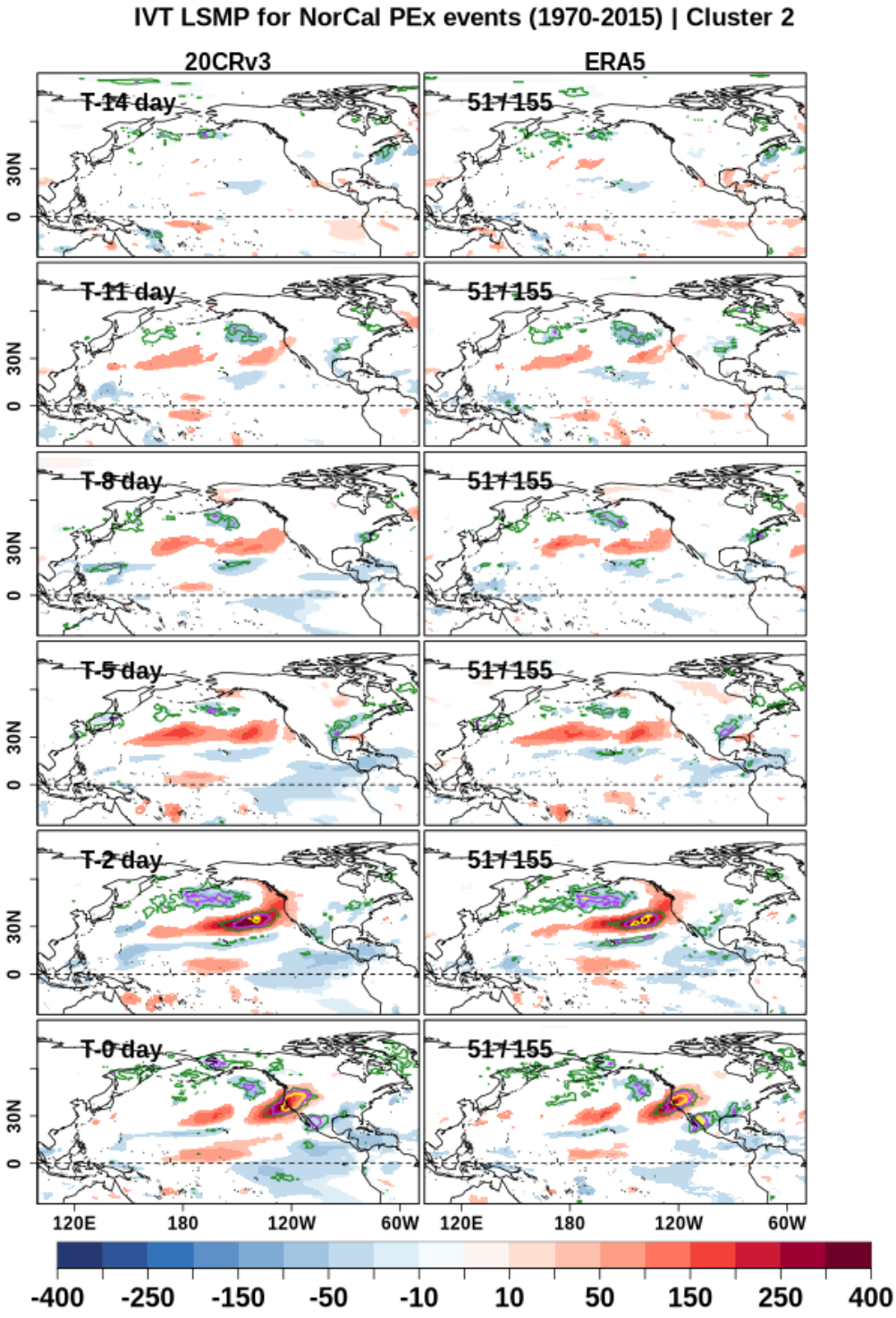

Figure S10: Same as in Fig. S9 but for cluster 2.

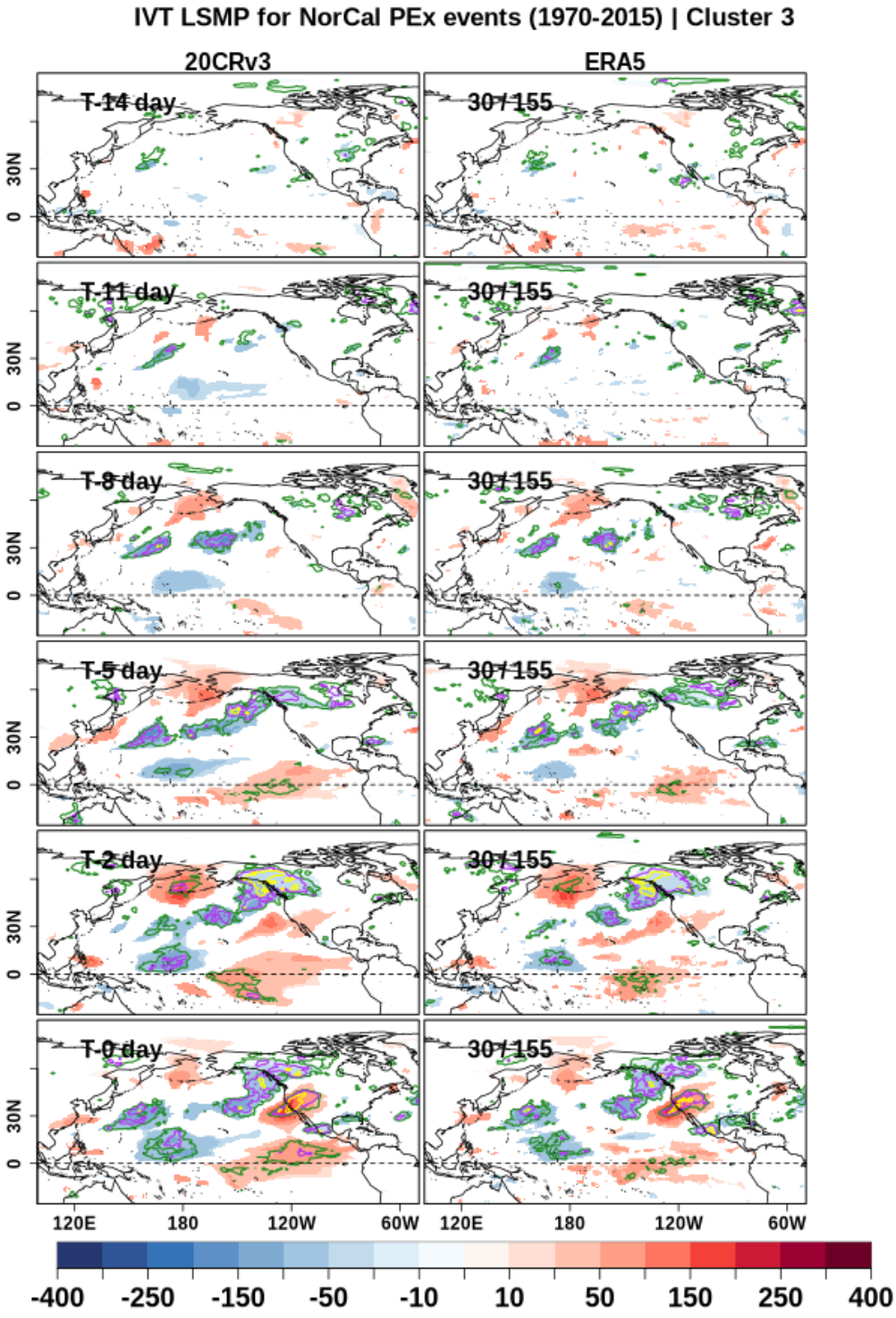

Figure S11: Same as in Fig. S9 but for cluster 3.

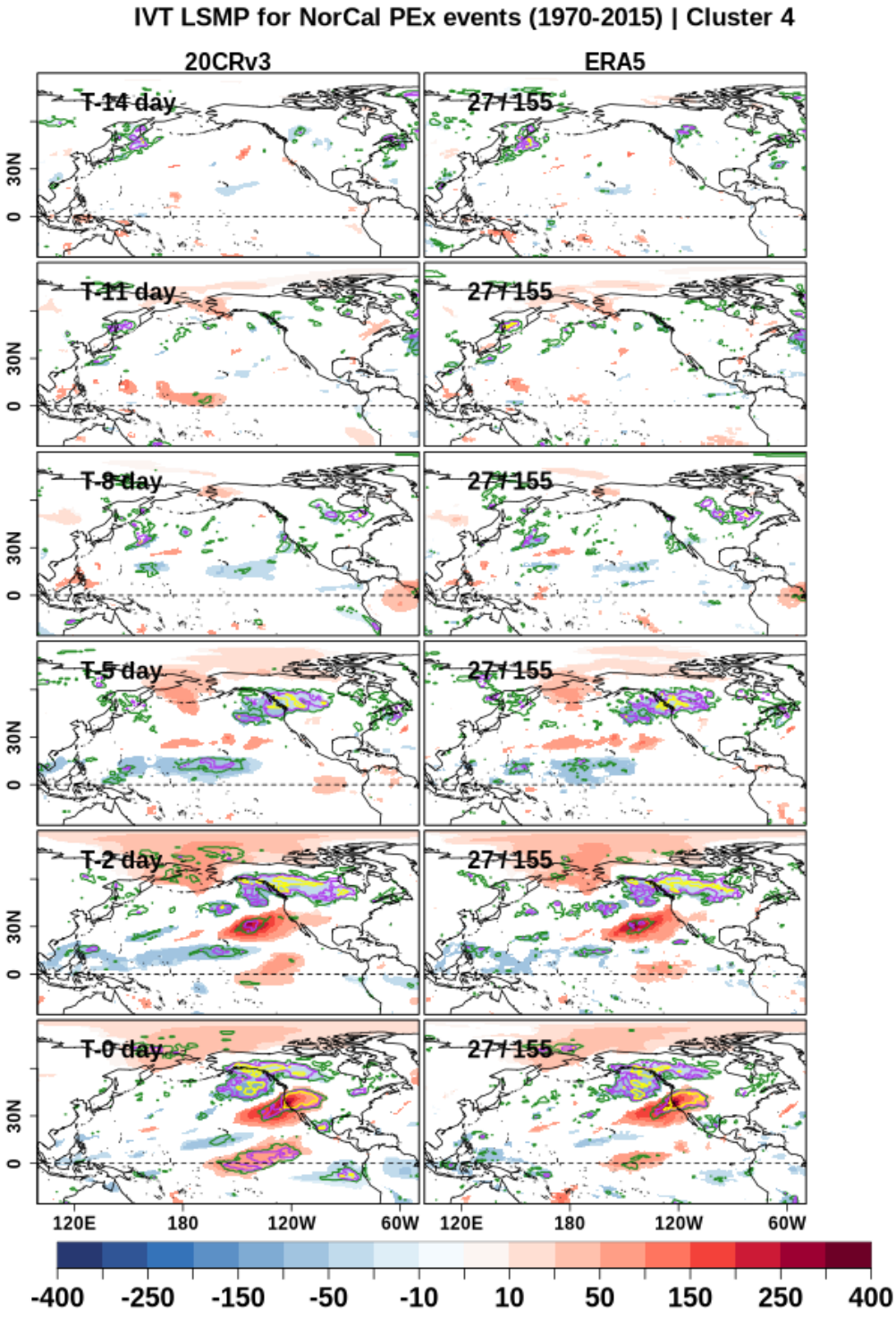

Figure S12: Same as in Fig. S9 but for cluster 4.

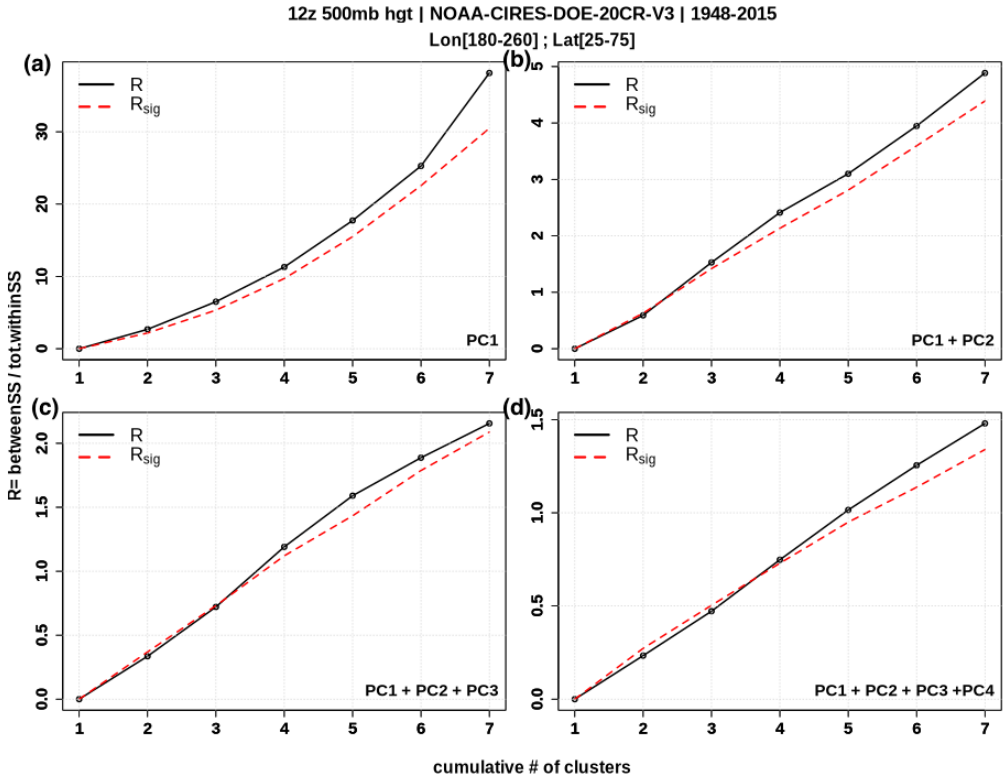

Figure S13: Variance ratio (R) for combinations of Za_{l2}^{500} PCs. The panels show the significance of Za_{l2}^{500} clusters for cluster numbers 1 to 7. Panels (a) - (d) show R computed from the first, first two, first three, and first four PCs, respectively. The X-axis shows the number of clusters for which the variance ratio (R) on the Y-axis is computed. The black curve shows variance ratio R computed from Za_{l2}^{500}. The red curve shows the 99^{th} percentile (R_{sig}) of the variance ratio computed from synthetic data generated using the Monte Carlo procedure. A cluster number is considered significant if $R > R_{sig}$.

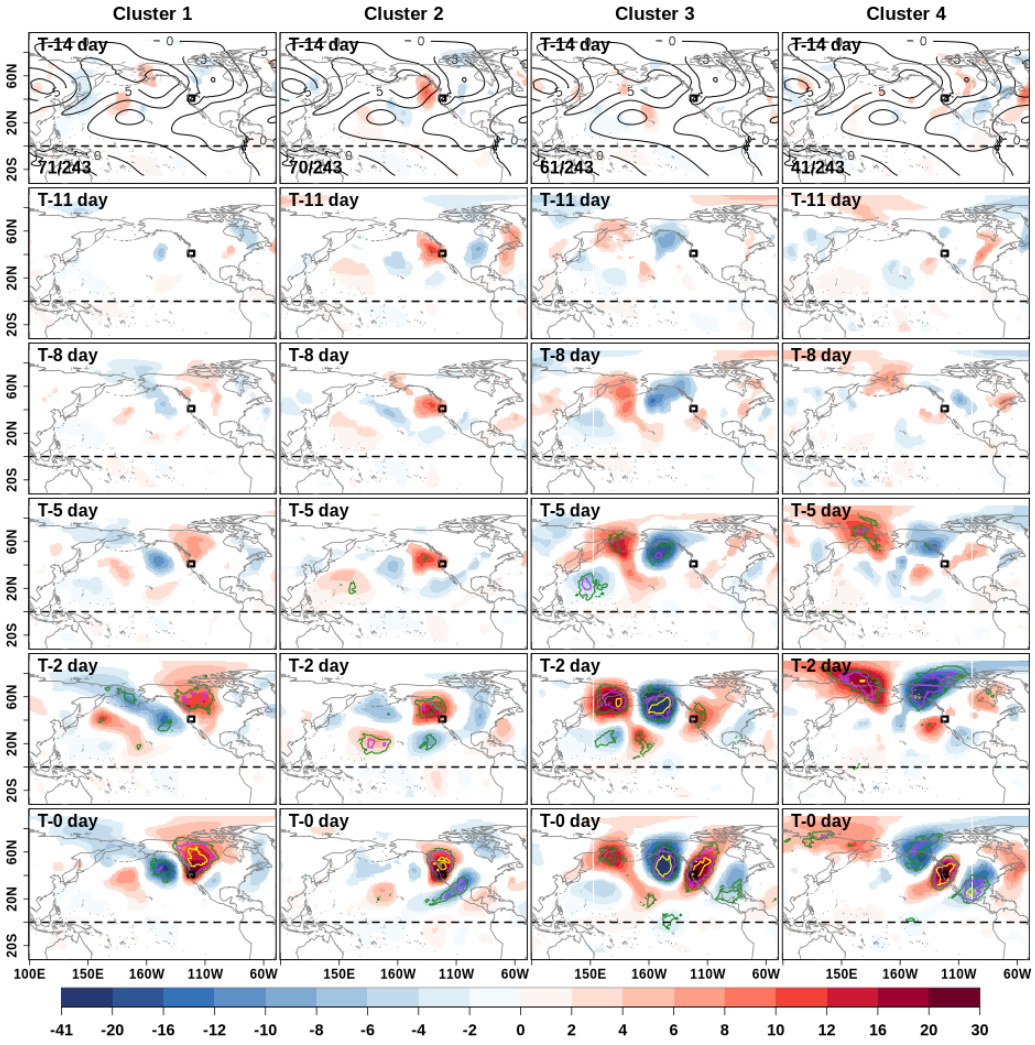

Figure S14: Evolution of 300 hPa meridional wind anomalies (unit: m/s). Shaded areas show anomalies significant at the 5% level. Contours show the consistency of the anomaly pattern. Green, magenta, and yellow contours show that at least 80%, 87.5%, and 95% of the cluster members have the same sign of anomalies, respectively. Solid black contours (contour interval: 5 m/s) in the top rows show the climatological meridional wind. The ratio in the lower-left corner in the top rows shows the number of events in that cluster divided by the total number of events. The black rectangle indicates the NorCal region.

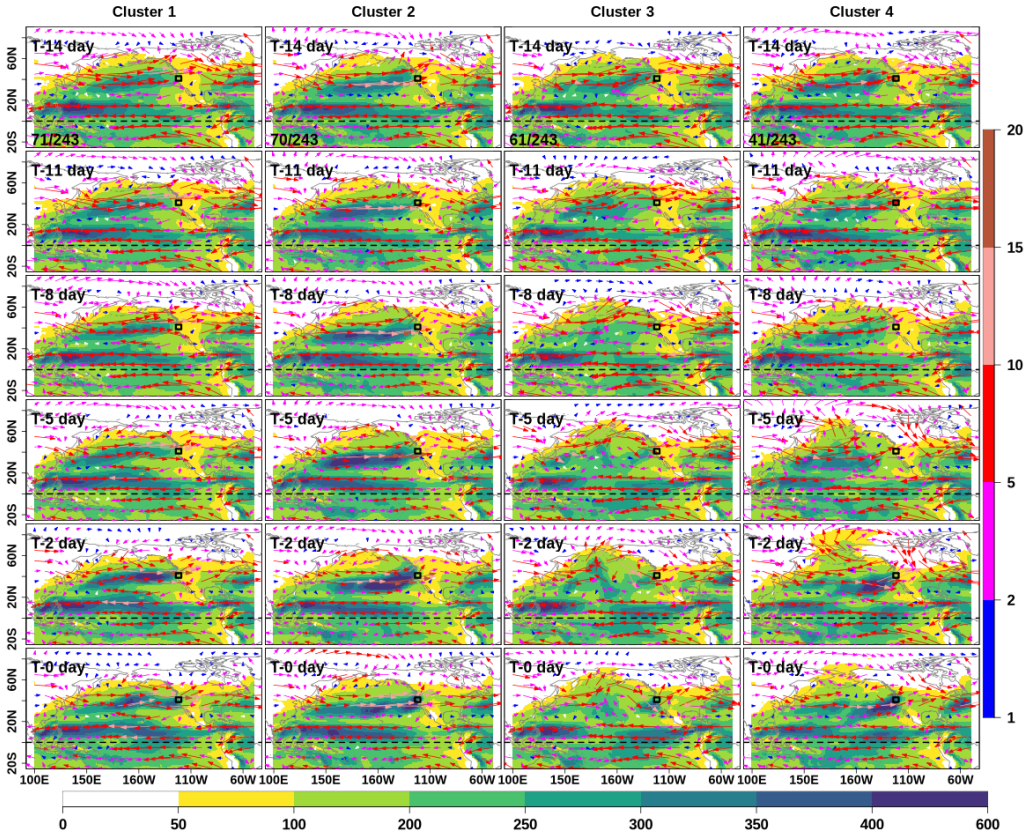

Figure S15: Evolution of the total integrated vapor transport (shading; unit: kg/m-s). The vectors show the 850 hPa wind (unit: m/s). The bottom color bar pertains to the IVT, and the vertical color bar to the 850 hPa wind.

Evolution of 850 hPa temperature and other anomalies

The evolution of the 850 hPa air temperature anomalies (Ta^{850}) for each of the four clusters is shown in Fig. S16. Ta^{850} is our archetype. Climatologically, lower and middle tropospheric temperature contours are approximately zonally-oriented with deviations due to relatively warmer air off the west coast and colder air on the east coast of the continents. Higher up, at 300 hPa, the meridional temperature gradient is weaker but similar to the lower levels (Supporting Information Fig. S18). The evolution of skin temperature (SkT; Supporting Information Fig. S19) differs from Ta^{850} by minimizing anomalies over the ocean. However, SkT has warm and cold anomalies over the tropical Pacific for clusters 2 and 3, respectively; but their possible links to ENSO are beyond the scope of this work.

Cluster 1 LSMP has three parts: 1) a warm anomaly largely confined to North America east of ∼120°W, 2) a cold anomaly from Alaska southeastward to just NW of NorCal, and 3) a mid-Pacific warm anomaly between 30-40°N. These three anomalies are present only two days before onset and occur throughout the troposphere. The primary cold anomaly near Alaska splits; the western portion remains over the Bering Sea while the eastern portion migrates along the Canadian west coast. Both motions can be anticipated from the expansion of the Aleutian low (e.g., Figs. 7 and 4) and advection by low level flow (e.g. Supporting Information Fig. S15). The continental warm anomaly can be similarly explained by southwesterly flow over that broad region. The mid-Pacific anomaly is also consistent with low level southeasterly flow. Both warm anomalies create upper level height anomalies shown in Fig. 4.

Cluster 2 has two anomalies in the troposphere: a warm anomaly arcing from Hawaii across the western CONUS into central Canada and a cold anomaly to the west. The most consistent part of the cold anomaly travels eastward by 30-50° degrees longitude in the two days leading up to onset. The western part of the warm anomaly initially has two parts at T-5 days: a part over Alaska and a part in the mid to eastern subtropical Pacific centered at ∼60°N and ∼20°N, respectively. The northern warm anomaly moves eastward to form the aforementioned arc. Both warm anomalies merging to form an arc is largely explainable from advection around the huge primary tropospheric low pressure anomaly along with enhanced pressure closer to the equator, visible in Figs. 4 and 7. The subtropical warm anomaly from Hawaii eastward sits where westerly IVT, characteristic of the midlatitudes, is unusually far south (∼25°N) where other clusters have easterlies (clusters 1 and 3) or weak westerlies (cluster 4). This flow arises from the increased pressure gradient created by pressure and height anomalies that are: negative unusually far south but positive even further south, near 15-20°N, visible in previous figures. Skin temperatures (Supporting Information Fig. S19) are also consistently warm there as well as along the equatorial Pacific from the dateline to Peru. Although it does not meet our consistency threshold (except a small area of Peru) the warm anomaly across the eastern equatorial Pacific is similar to the sea surface temperature pattern during an El Niño. Furthermore, the warm anomaly over the ocean along the west coast of North America that is accompanied by a cold anomaly in the central North Pacific resembles the positive phase of the Pacific decadal oscillation (PDO) pattern. Having this pattern, even though the ocean resists temperature changes, might suggest a preference for this cluster during positive PDO and El Nino.

In cluster 3, the 850 hPa temperature anomaly pattern has three parts that largely follow from flow around the two SLPa anomalies (Fig. 7). The west side of the huge pressure ridge drives subtropical air northward warming the northern Pacific and Bering Sea. Between that ridge and the low pressure at the NW CONUS cold air is driven southward from western Canada, across the Gulf of Alaska to southwest of NorCal. Finally, just prior to onset, a warm anomaly develops over Mexico. Unlike the prior two clusters, all three anomalies are essentially stationary over a week. This tri-polar temperature anomaly pattern generates three of the anomalies seen in 500hPa streamfunction shown in Fig.

4. The temperature anomalies at 500 hPa are similar to the lower elevation pattern except for a cold anomaly SW of Hawaii that matches 500hPa patterns in Figs. 3 and 4. The skin temperature (Supporting Information Fig. S19) is somewhat similar to 850 hPa over the land masses but also has some notable oceanic anomalies: an intense warm anomaly south of the Aleutians and an equatorial eastern Pacific cold anomaly. The latter is suggestive of "La Niña" conditions. At 300 hPa, the anomalies are similar and largely coincident to those at 500 hPa (also 850h Pa) but with smaller magnitudes.

The key characteristic in cluster 4 in Fig. S16 is the deep, stationary, warm anomaly covering Alaska, Bering Sea, and much of the Arctic Ocean. The broad extent invites comparison with future climate simulations showing amplified Arctic warming. It would be instructive to check if cluster 4 occurs more frequently in a warming world. This anomaly is also quite strong at 500hPa and consistent with low-level flow implied by SLPa. Over western Canada, an intense cold anomaly in Ta^{850} (and SkT) develops a few days before onset. At 500 hPa, this cold anomaly is less prominent (Supporting Information Fig. S17). Also developing shortly before onset is a highly consistent warm anomaly extending from the PEx area southwestward into the subtropical Pacific as far as Hawaii. South of 40°N, this latter warm anomaly has similar extent to cluster 2, except it is slightly further south over the ocean. Unlike cluster 2, this more southern warm anomaly only develops just before onset. As for the other clusters, the 300 hPa temperature anomaly patterns (Supporting Information Fig. S18) are similar to those at 500 and 850 hPa, but with smaller magnitudes. The Ta^{850}, Ta^{500}, and SkT patterns north of ∼45°N are strongest at T-2 and largely opposite-signed from cluster 1, though close to the PEx region at onset their temperature anomalies match.

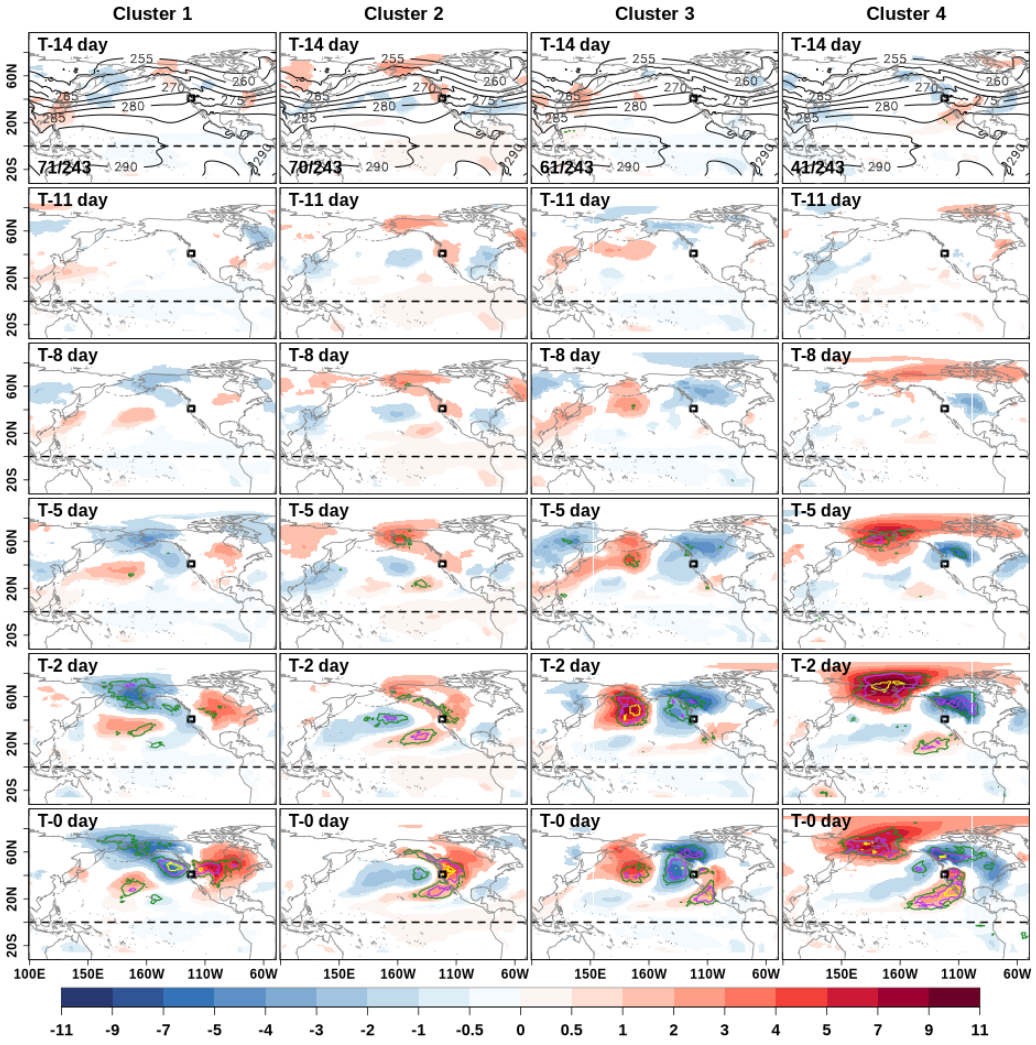

Figure S16: Evolution of 850 hPa air temperature anomalies (unit: K). Shaded areas show anomalies significant at the 5% level. Contours show the consistency of the anomaly pattern. Green, magenta and yellow contours show that at least 80%, 87.5%, and 95% of the cluster members have the same sign of anomalies, respectively. Solid black contours (contour interval: 5 K) in the top row show the climatological 850 hPa air temperature. The ratio in the lower-left corner of each top row panel shows the number of events in that cluster divided by the total number of events. The black rectangle indicates the NorCal region. The dashed line marks the equator.

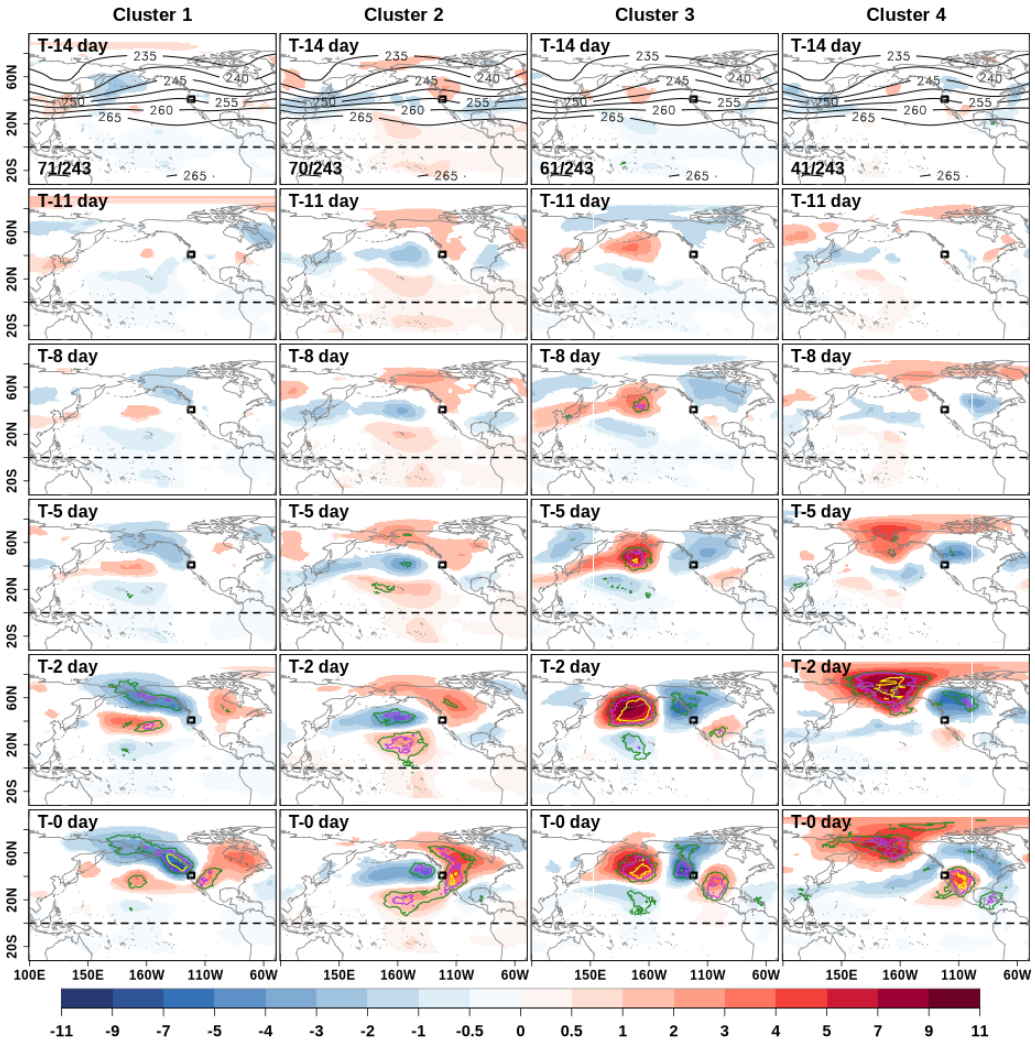

Figure S17: Same as Fig. S16 but for the evolution of the 500 hPa air temperature anomaly (unit: K). Solid black contours (contour interval: 5K) in the top rows show the climatological 500 hPa air temperature anomaly.

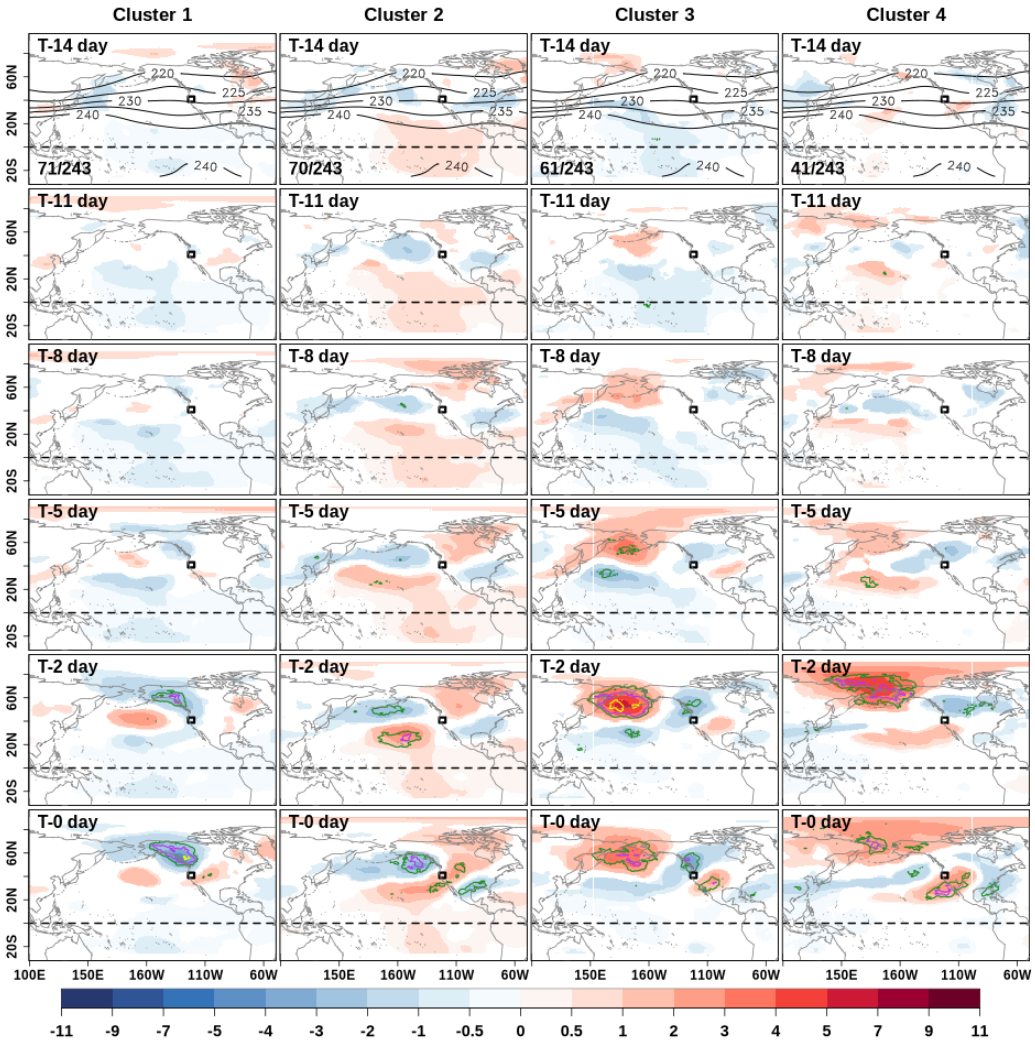

Figure S18: Same as Fig. S16 but for the evolution of the 300 hPa air temperature anomaly (unit: K). Solid black contours (contour interval: 5 K) in the top rows show the climatological 300 hPa air temperature anomaly.

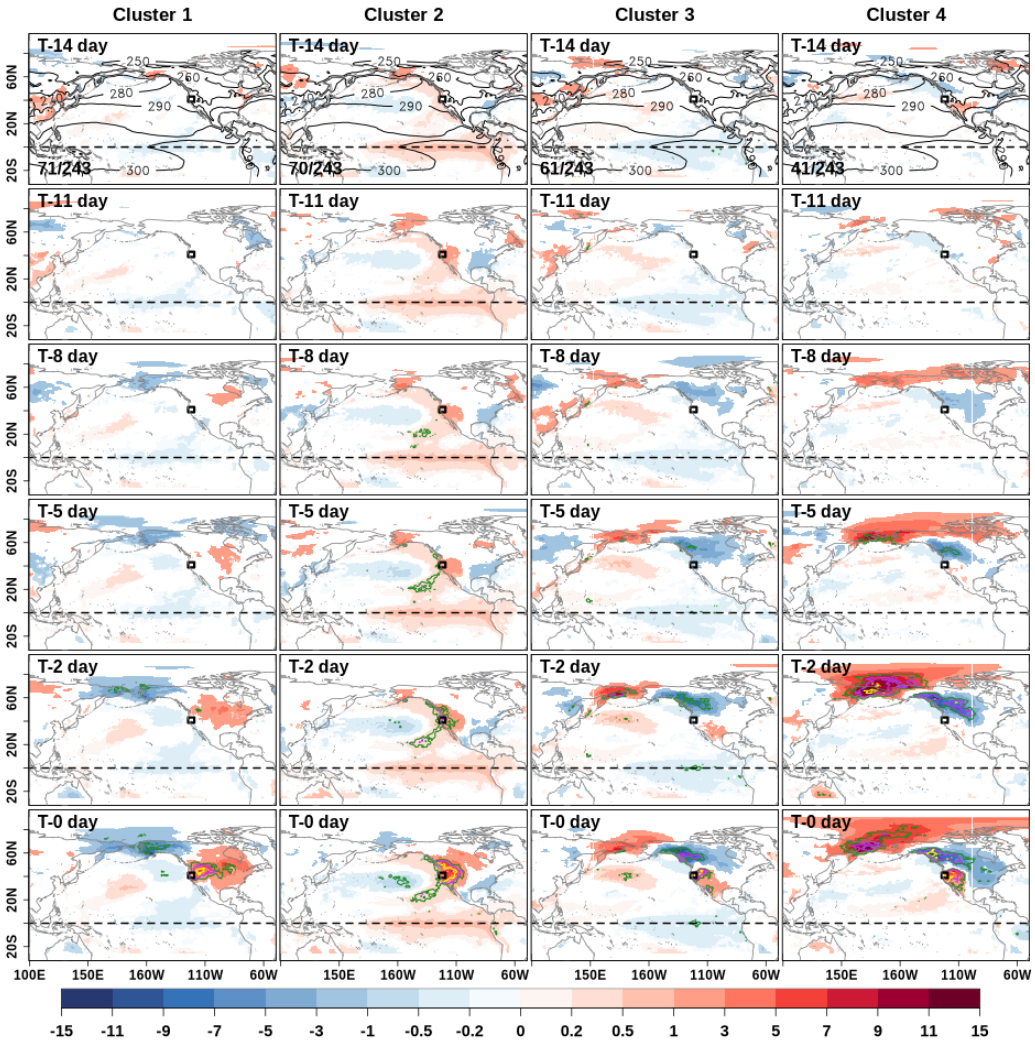

Figure S19: Same as Fig. S16 but for the evolution of the skin temperature anomalies (unit: K). Solid black contours (contour interval: 10 K) in the top rows show the climatological skin temperature anomalies.

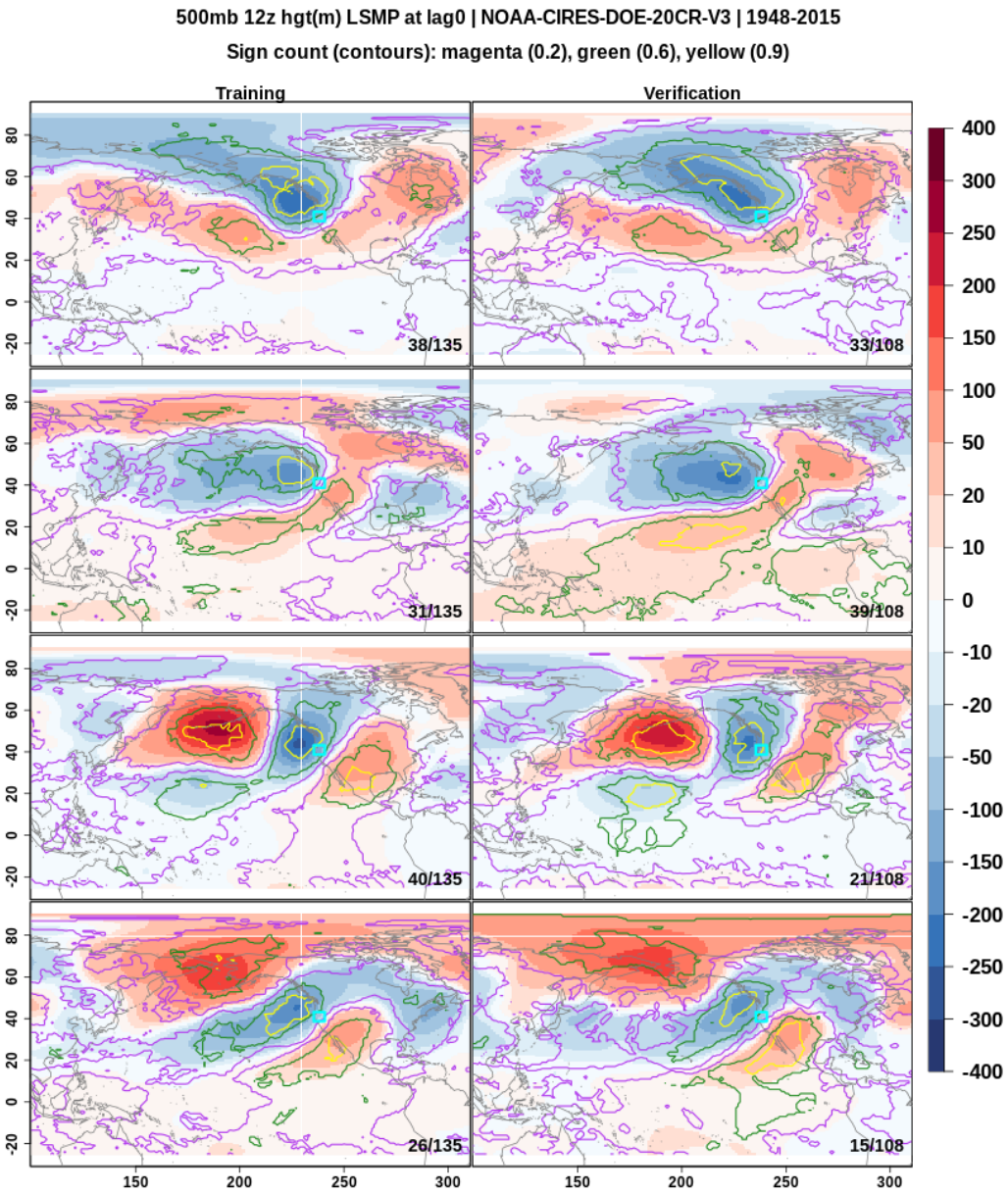

Figure S20: LSMP clusters for lag 0 500mb geopotential height anomalies during months November-March. The left panel shows the LSMP for the training period (1948-1982) and the right panel shows the LSMP for the verification period (1982-2015). Unit: m.